photonics

Article

A 5 kW Nearly-Single-Mode Monolithic Fiber Laser Emitting at ~1050 nm Employing Asymmetric Bi-Tapered Ytterbium-Doped Fiber

Xiangming Meng [1], Fengchang Li [1], Baolai Yang [1,2,3,*], Peng Wang [1,2,3], Zhiping Yan [1,2,3], Yun Ye [1,2,3], Xiaoming Xi [1,2,3], Hanwei Zhang [1,2,3], Zhiyong Pan [1,2,3], Xiaolin Wang [1,2,3,*] and Fengjie Xi [1,2,3]

1 College of Advanced Interdisciplinary Studies, National University of Defense Technology, Changsha 410073, China
2 Nanhu Laser Laboratory, National University of Defense Technology, Changsha 410073, China
3 Hunan Provincial Key Laboratory of High Energy Laser Technology, National University of Defense Technology, Changsha 410073, China
* Correspondence: yangbaolai@nudt.edu.cn (B.Y.); wxllin@nudt.edn.cn (X.W.)

Abstract: Limited by stimulated Raman scattering (SRS), amplified spontaneous emission (ASE) and transverse mode instability (TMI), it is challenging to achieve high-power laser output in ytterbium-doped fiber (YDF) lasers with operating wavelengths less than 1060 nm. In high-power fiber lasers, bi-tapered YDF can provide a balance between the suppression of SRS and TMI. In this work, we designed and fabricated a new double-cladding asymmetric bi-tapered YDF to suppress ASE and SRS in the 1050 nm monolithic fiber laser. The asymmetric bi-tapered YDF has an input end with a core/cladding diameter of ~20/400 µm, a middle section with a core/cladding diameter of ~30/600 µm and an output end with a core/cladding diameter of ~25/500 µm. The working temperature of the non-wavelength-stabilized 976 nm laser diodes was optimized to improve the TMI threshold. An output power of over 5 kW with an efficiency of 83.1% and a beam quality factor M^2 of about 1.47 were achieved. To the best of our knowledge, this represents the highest power nearly-single mode in 1050 nm fiber lasers. This work demonstrates the potential of asymmetric bi-tapered YDF for achieving a high-power laser with high beam quality in 1050 nm fiber lasers.

Keywords: high-power fiber laser; asymmetric bi-tapered ytterbium-doped fiber; stimulated Raman scattering; transverse mode instability; amplified spontaneous emission

Citation: Meng, X.; Li, F.; Yang, B.; Wang, P.; Yan, Z.; Ye, Y.; Xi, X.; Zhang, H.; Pan, Z.; Wang, X.; et al. A 5 kW Nearly-Single-Mode Monolithic Fiber Laser Emitting at ~1050 nm Employing Asymmetric Bi-Tapered Ytterbium-Doped Fiber. *Photonics* **2023**, *10*, 1158. https://doi.org/10.3390/photonics10101158

Received: 10 September 2023
Revised: 7 October 2023
Accepted: 13 October 2023
Published: 16 October 2023

1. Introduction

High-power fiber lasers (operating at wavelengths below 1060 nm) have important applications in spectral combining and nonlinear frequency conversion [1–3]. As a type of spectral combining technology, dichroic mirrors combining refers to the application of a dispersive element to combine multiple lasers by refraction and reflection [4,5]. Dichroic mirror combining technology can achieve high brightness, high stability, and high efficiency in medium-power output. The beam combining technology places an output power demand on fiber lasers operating at different working wavelengths. In fact, the spectral range of ytterbium-doped fiber lasers spans from 960 to 1200 nm [6]. Fiber lasers operating at wavelengths below 1060 nm offer the advantage of suppressing transverse mode instability (TMI) due to lower quantum defect heating and a stronger gain saturation effect [7]. However, fiber lasers operating at wavelengths below 1060 nm face challenges in achieving high-power output due to their relatively smaller net gain and limitations imposed by amplified spontaneous emission (ASE). Fiber lasers operating in the wavelength range of 1060 to 1080 nm have a larger net gain, which makes them less susceptible to ASE and more capable of achieving high-power output. However, TMI and nonlinear effects such as stimulated Raman scattering (SRS) need to be carefully considered.

In recent years, fiber lasers operating at wavelengths below 1060 nm have been reported by multiple research institutions [8–16]. In 2016, Naderi et al. constructed a narrow linewidth fiber amplifier at 1034 nm with an output power of 1 kW [9]. The length of the gain fiber was optimized to suppress ASE. Also in the same year, Sun et al. reported a 1030 nm fiber amplifier employing master oscillator power amplifier (MOPA) structure [10]. A maximum output power of 1.01 kW with an optical-to-optical (O–O) efficiency of 81% was achieved. In 2021, Xu et al. realized 2.4 kW of output power at 1045 nm using a MOPA structure [15]. An 8.5 m long ytterbium-doped fiber (YDF) was applied to suppress ASE. In this structure, higher power outputs were difficult to realize limited by SRS. In 2022, Zheng et al. built a 1050 nm fiber laser using pump-sharing structure with an output power of 3.1 kW [16]. When demonstrating fiber lasers with a wavelength below 1060 nm, several factors such as ASE, TMI, and nonlinear effects need to be considered and effectively suppressed [17,18].

In fiber lasers based on large mode area (LMA) YDF, the variation of the longitudinal structure of the active fibers has gradually gained attention. These novel active fibers have non-uniform geometry in the longitudinal direction [19,20]. The small core section can control the beam propagation mode, which is advantageous for suppressing TMI [21]. The large core section can increase the mode field area, which is beneficial for mitigating SRS [22]. Furthermore, due to the non-uniform longitudinal geometry, ASE can also be suppressed [19,23]. Since 2008, an extensive amount of theoretical and experimental research has been conducted on the active fibers with longitudinal structural variations with the tapered fiber as a representative example [19–28]. In 2018, Fedotov et al. utilized a tapered fiber with a core diameter of 96 μm to demonstrate a linearly polarized continuous wave (CW) laser operating emitting at 1040 nm [26]. This fiber laser achieved an output power of 70 W. In 2021, Zeng et al. constructed a monolithic fiber amplifier using a spindle-shaped YDF with an output power of 5 kW at 1070 nm [28]. The core/cladding diameter at both ends is 27/410 μm, while in the middle, it measures 39.5/600 μm. Fiber lasers operating at the wavelength around 1080 nm achieved nearly-single-mode output levels of 6 kW as early as 2008 [29]. In 2009, IPG Photonics reported a counter-pumped fiber laser with a power level of around 10 kW [30]. Through optimization of the gain fiber and pump sources, the company further reported a nearly-single-mode fiber laser output of 20 kW in 2013 [31]. Active fibers with a non-uniform longitudinal geometry can achieve an output power of over 5 kW in conventional wavelength ranges, but the novel fibers are less studied on 1050 nm fiber lasers. Currently, the output power of a nearly-single-mode 1050 nm CW fiber laser remains at the level of 3 kW, and the power scaling of fiber lasers operating at wavelengths below 1060 nm needs to be boosted [13,16].

In this manuscript, we constructed a counter-pump monolithic fiber laser amplifier employing an asymmetric bi-tapered YDF. A specially designed 13 m long asymmetric bi-tapered YDF is applied to suppress the ASE and SRS. Non-wavelength-stabilized 976 nm laser diodes (LDs) have been utilized as the pump sources. In order to raise the TMI threshold, the working temperature of the LDs was optimized. By combining the suppression of SRS, TMI and ASE, we successfully achieved a 5 kW nearly-single-mode laser emitting at 1050 nm with high SRS suppression ratio of ~30 dB. At the maximum power, the beam quality factor M^2 is 1.47 with an O–O efficiency of 83.1%.

2. Experimental Setup

The fiber laser based on the counter-pumped structure, as shown in Figure 1a, consists of a seed and an amplifier stage. A counter-pumped oscillator is applied to the seed, which can provide an output power of approximately 250 W. The resonator of the seed is composed of a pair of fiber Bragg gratings (FBGs) with a center wavelength of 1050 nm. The diameters of the core and cladding of the FBGs are 20 μm and 400 μm, respectively. The output coupler fiber Bragg grating (OC-FBG) features a reflection rate of 9.7% and a bandwidth of 2.05 nm. On the other hand, the high reflectivity fiber Bragg grating (HR-FBG) exhibits a reflection rate of 99% and a bandwidth of 4 nm. The seed utilizes a conventional

YDF with a core/cladding diameter of 20/400 µm as the gain fiber. To suppress the impact of ASE in the 1050 nm fiber laser, the length of the YDF has been optimized to 4.8 m. The pump absorption coefficient of the YDF at the wavelength of 976 nm is 1.26 dB/m. The output fiber of the OC-FBG is connected to a (2 + 1) × 1 side-pumped combiner. The pump input fiber of the side-pumped combiner is connected to two wavelength-stabilized 976 nm LDs with a power of 250 W each. The output fiber of the HR-FBG is linked to a commercial cladding light stripper (CLS-1), with the opposite end of the CLS angled at ~8°. The signal fiber of the side-pumped combiner is spliced to the bi-tapered YDF of the amplifier stage. The core/cladding diameter of the bi-tapered YDF at the input and output fiber is 20/400 µm and 25/500 µm. The core/cladding diameter of the bi-tapered YDF in the middle section is 30/600 µm. To suppress TMI, the bi-tapered YDF is coiled in a fiber grove with a bending diameter of 9.5 cm to 13.5 cm. The output end of the bi-tapered YDF is spliced to an (18 + 1) × 1 backward pump/signal combiner (PSC). The output fiber of the PSC has a core/cladding diameter of 25/500 µm, which ensures a matched fusion with the bi-tapered YDF thus suppressing higher-order modes (HOMs) from being excited. Eighteen non-wavelength-stabilized 976 nm LDs are connected to the pump fiber of the PSC, delivering a pump power of ~5.8 kW. The core/cladding diameter of the pump fiber is 135/155 µm. The signal fiber of the PSC is linked to a CLS-2, which filters out residual pump light. The output fiber of CLS-2 is spliced to a home-made quartz block holder (QBH). The delivery fiber from PSC output to QBH has a length of 3 m and a core/cladding diameter of 25/250 µm.

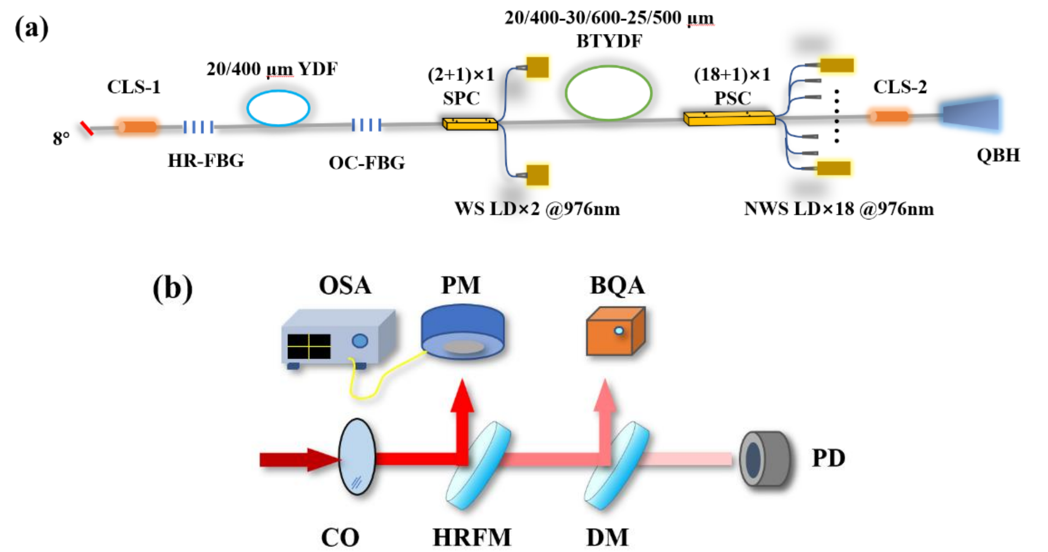

Figure 1. (**a**) Experimental schematic of 1050 nm monolithic fiber laser amplifier (CLS: cladding light stripper; HR–FBG: high–reflectivity fiber Bragg grating; OC–FBG: output coupler fiber Bragg grating; YDF: Ytterbium–doped fiber; SPC: side–pump combiner; BTYDF: bi–tapered YDF; PSC: pump/signal combiner; WS LD: wavelength–stabilized laser diode; NWS LD: non–wavelength–st–bilized laser diode; QBH: quartz block head); (**b**) schematic diagram of the testing system (CO: co–limator; OSA: optical spectrum analyzer; PM: power meter; HRFM: high–reflectivity flat mirror; BQA: beam quality analyzer; PD: photodetector).

The output laser from the QBH is received by a testing system. A schematic diagram of the testing system is shown in Figure 1b. The testing system consists of a 15 kW power meter (PM), an optical spectrum analyzer (OSA), a four-channel high-speed photodetector (PD), and a beam quality analyzer (BQA). The high-power laser through collimator (CO) is divided into two beams using a mirror coated with a high-reflectivity flat mirror (HRFM). The reflected light is received by the PM to test the output power. The scattered light signal is employed to test the spectra. The transmitted light is separated by a dichroic mirror (DM), and the reflected light is received by the BQA to test the beam quality. To analyze the temporal characteristics of the output laser, the PD with a bandwidth of 1 GHz is utilized to capture the temporal signal.

The preparation of the bi-tapered YDF mainly consists of two key steps: fiber preforms fabrication and fiber drawing. The main process for the preparation of the bi-tapered YDF preform includes cleaning of the reaction tube, deposition of the barrier layer, deposition of the porous layer, solution doping, drying and dehydration, high-temperature vitrification, and diameter reduction. It is worth noting that the mainstream fiber fabrication technique currently employed is the modified chemical vapor deposition (MCVD) process [32]. After obtaining the fiber preform that meets the requirements, the next step is fiber drawing. The asymmetric bi-tapered YDF maintains a constant core–cladding ratio along the longitudinal direction. As the core diameter and cladding diameter of the fiber increase proportionally, a variable-speed drawing technique is used to achieve fiber drawing. The main steps of fiber drawing include sleeving, coating, and UV curing treatment. The 2D schematic diagram of the home-made double-cladding asymmetric bi-tapered YDF is shown in Figure 2a, and the 3D schematic is shown in Figure 2b. The bi-tapered YDF can be divided into five sections. In our experiment, the input and output ends of the YDF are denoted as S1 and S5, and the length is both 2 m. The middle section S3 is the large-size region with a length of 3 m. S2 and S4 are transition regions, and the lengths are 4 m and 2 m, respectively. The coating diameter remains constant along the fiber direction at 710 µm. The design of the total length of active fiber considers the suppression of SRS and ASE. The cladding pump absorption coefficient of the bi-tapered YDF at 976 nm is 1.3 dB/m. Compared to a conventional symmetric bi-tapered YDF with a small-core diameter of 25/400 µm [24], the asymmetric bi-tapered YDF with a core/cladding diameter of 25/500 µm has a larger effective mode field area at the output end, enabling the effective suppression of SRS. Moreover, compared to a conventional symmetric bi-tapered YDF with a small-core diameter of 27/410 µm [28], the input end of the asymmetric bi-tapered YDF with a core/cladding diameter of 20/400 µm has a smaller core size. The small core diameter allows fewer transmission modes to propagate, which is beneficial for maintaining the beam quality and achieving nearly-single-mode laser output.

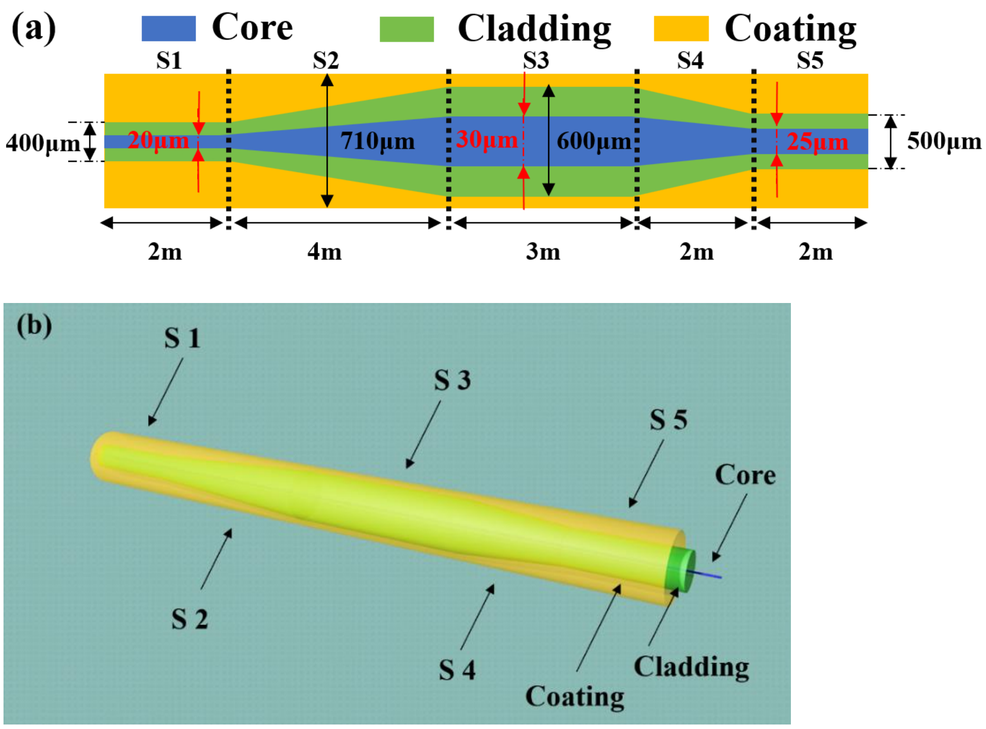

Figure 2. (**a**) Two-dimensional (2D) schematic diagram of the longitudinal structure of the bi-tapered YDF; (**b**) 3D schematic diagram of the longitudinal structure of the bi-tapered YDF.

3. Results and Discussion

3.1. TMI Mitigation by Optimizing Working Temperature of Pump Source

Fiber lasers pumped by non-wavelength-stabilized 976 nm LDs possess a higher TMI threshold compared to those pumped by wavelength-stabilized 976 nm LDs [33,34]. In our experiments, non-wavelength-stabilized 976 nm LDs were chosen to be used as the pump source for the amplifier stage in order to suppress TMI. The output characteristics of the fiber amplifier were evaluated using a bi-tapered YDF at a working temperature of 20 °C. The initial seed power is 155 W. As shown in Figure 3a, the output power of the fiber amplifier is 4710 W when the pump power is 5710 W with an O–O efficiency of 86.0%. The nonlinearity of the efficiency curve originates from the non-wavelength-stabilized LDs pumping. The center wavelength of the non-wavelength-stabilized LDs changes with the pump current. The variation in pumping wavelength results in different absorption levels of the pumped light by the YDF, leading to varying O-O efficiencies at different power points. Therefore, the ups and downs of the efficiency curves are shown.

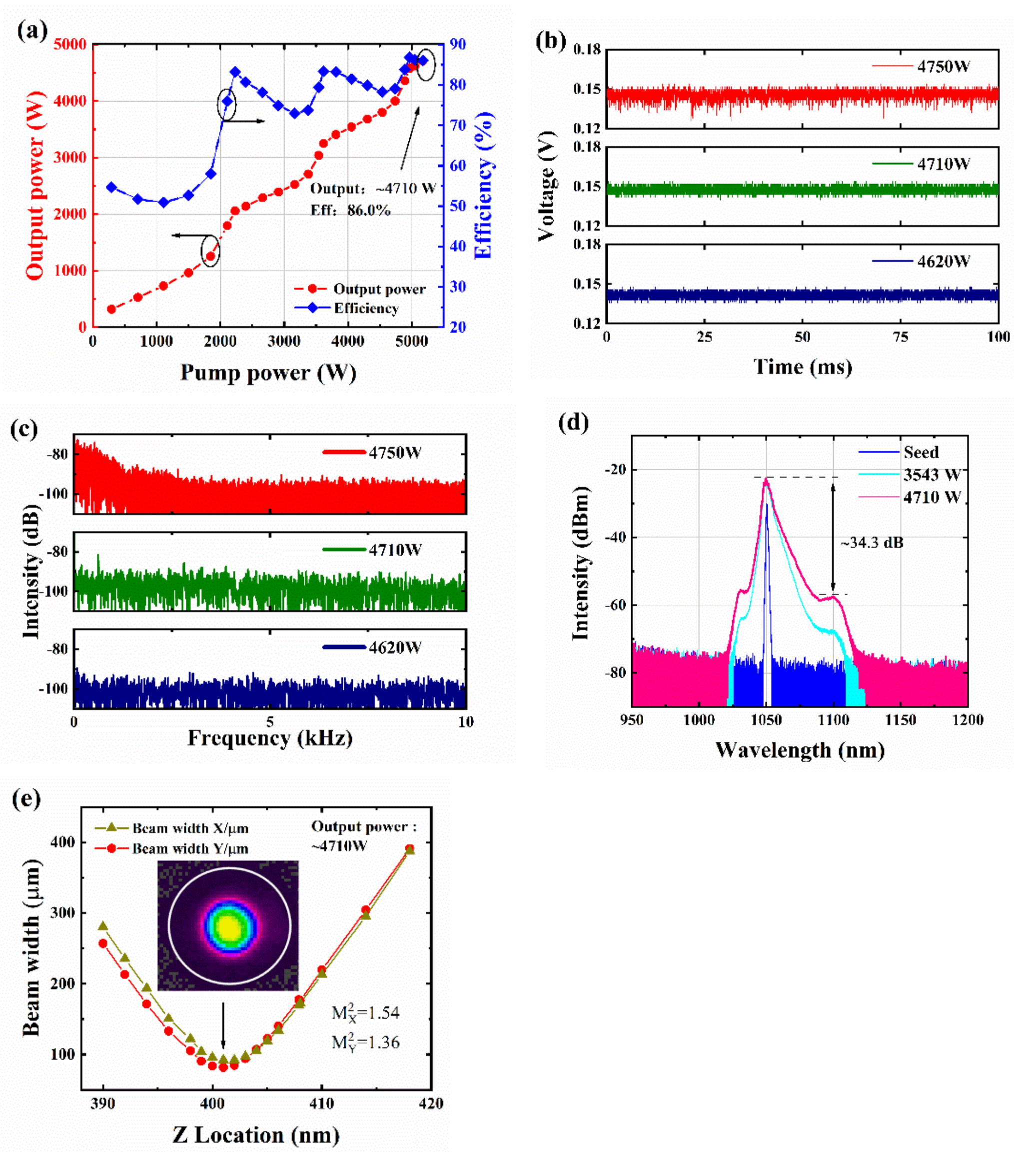

Figure 3. (**a**) Output power and conversion efficiency corresponding to different pump powers of fiber amplifier at working temperature of 20 °C; (**b**) temporal signal at power levels around the TMI threshold; (**c**) the corresponding Fourier spectra; (**d**) output spectra at different output powers; (**e**) beam quality at 4710 W (inset: a beam profile of the output laser).

Figure 3b,c show the normalized temporal signals from the PD and the corresponding Fourier spectra around the TMI threshold in the fiber laser with asymmetric bi-tapered YDF. When the output power is 4710 W, fluctuations can be observed in both the temporal signal and the Fourier spectrum. When the output power reaches 4750 W, the fluctuations in the temporal signal became more pronounced, and severe fluctuations can be seen in the Fourier spectrum within the range of 0–2.5 kHz. This fluctuation observed in both the time and frequency domains is a characteristic indication of TMI [35]. The spectrum when TMI occurs is shown in Figure 3d, which the signal-to-noise ratio (SNR) is ~34.3 dB. The spectra at the seed and output power of 3543 W are also depicted in Figure 3d. The high SNR of the spectrum is due to the good performance of the asymmetric bi-tapered YDF. The beam quality at the TMI threshold is shown in Figure 3e, where the beam quality factors M^2 for the X and Y directions are 1.54 and 1.36, respectively.

To achieve higher power laser output, it is important to further enhance the TMI threshold. The center wavelength of the non-wavelength-stabilized LDs demonstrates a significant variation with temperature, which presents an opportunity for optimizing the pumping wavelength. Figure 4a displays the pump wavelength of the LD tested at different pump currents at 15 °C. The total pump power of each LD was measured to be 330 W. When the pump current was increased from 4 to 28 A, the pump wavelength shifted from 961.24 to 972.91 nm. Figure 4b illustrates the variation in the central wavelength of the non-wavelength-stabilized 976 nm LDs at different working temperatures with varying currents. As the working temperature of the LD decreased from 20 to 15 °C, the pump wavelength drifted from 975.07 to 972.91 nm for the LDs at a maximum operation current of 28 A. It is important to note that the pump current has a more pronounced effect on the pump wavelength. Limited by the total pump power, optimizing the working temperature of the LDs is essential for raising the TMI threshold.

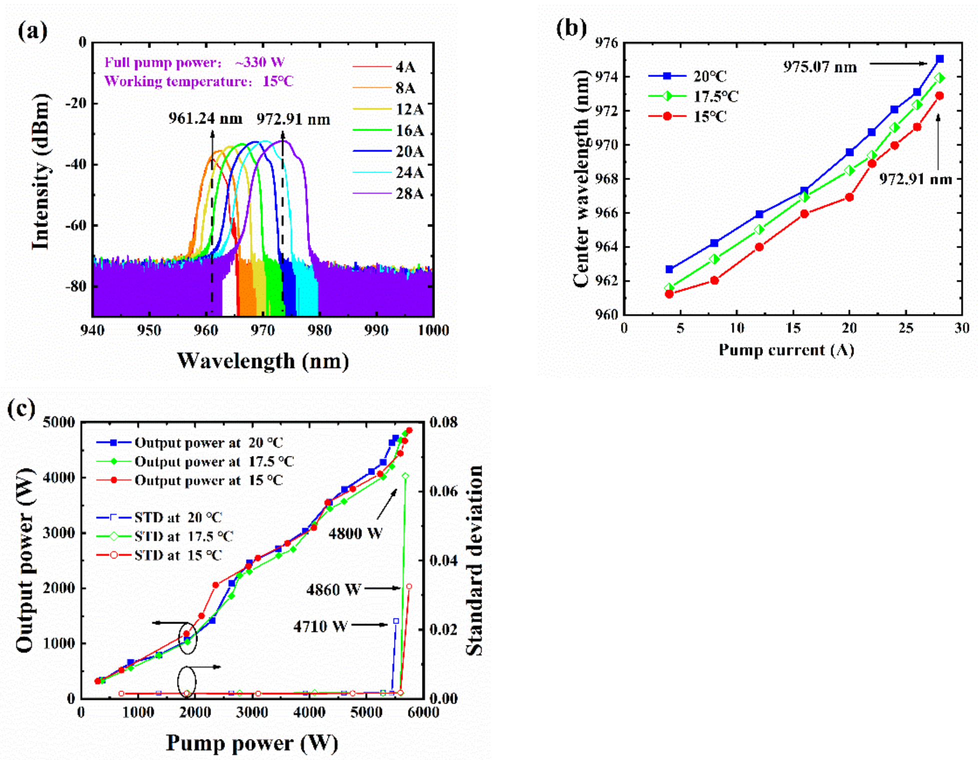

Figure 4. (**a**) The pump wavelength of the LD tested at different pump currents at 15 °C; (**b**) the variation curve of center wavelength of non–wavelength–stabilized 976 nm LDs with pump current at different working temperatures; (**c**) the variation curve of output power and STD with pump power at different working temperatures.

The output power of the fiber laser was measured at working temperatures of 20 °C, 17.5 °C, and 15 °C for the LDs, as shown in Figure 4c. The TMI threshold at 20 °C was determined to be 4710 W, while at 15 °C, it was raised to 4860 W, resulting in an increase of approximately 150 W in the TMI threshold. To quantitatively determine the threshold of TMI, the standard deviation (STD) of the temporal signals was calculated at different output powers [36–38]. The threshold for TMI was defined as the output power corresponding to when the STD exceeded 0.01, which is a commonly used determination method nowadays [38,39]. By optimizing the working temperature of the pumping source, we successfully increased the TMI threshold to 4860 W.

3.2. Power Scaling of the Monolithic Fiber Laser by Enhancing Seed Power

To achieve further power scaling, the seed power was increased from 155 to 253 W. The characteristics of different seed powers were tested as shown in Figure 5. The full-width at half-maximum (FWHM) is 0.86 nm when the seed power is 155 W. When the seed power is 253 W, the FWHM is 1.07 nm. The beam quality factor M^2 is 1.49/1.32 for the seed power of 155 W and 1.49/1.30 for the seed power of 253 W. The change in the beam quality of the seed is not significant, but the FWHM of the seed has a broadening phenomenon. The spectral broadening of the seed also contributes to increasing the temporal stability of the seed [39]. Combined with the conclusion in the previous subsection that a lower working temperature of the pump source is favorable to increase the TMI threshold, we chose a working temperature of 253 W for the seed and 15 °C for the amplification stage pumping source for the high-power experiments. The temperature of the other devices is 20 °C.

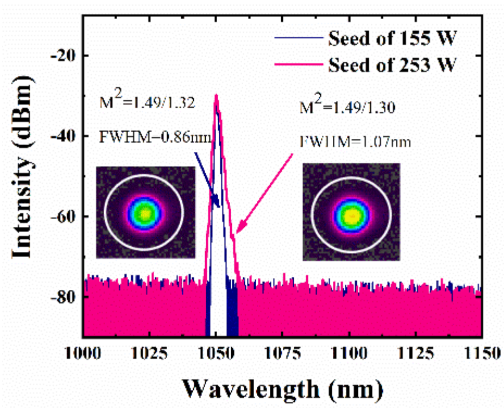

Figure 5. Spectra of different seed powers (inset: the beam profiles of the seed laser).

The output characteristics of the fiber laser employing an asymmetric bi-tapered YDF are illustrated in Figure 6. At a pump power of 5750 W, the output power reaches 5030 W, as displayed in Figure 6a. This power corresponds to an O-O efficiency of 83.1%. The high efficiency of the fiber laser can be attributed to the pump-sharing structure [16]. In this configuration, there is no isolation device (such as a CLS) between the seed and the amplifier stage. As a result, the unabsorbed pump light from the active fiber of the amplifier stage can enter the YDF of the seed through the side-pumped combiner, leading to an increased O-O efficiency. The corresponding spectra for different output powers are depicted in Figure 6b. When the output power is 5030 W, the center wavelength of the output laser is 1049.98 nm with an FWHM of 4.46 nm. At this power level, the Raman light has a center wavelength of ~1100 nm and an intensity ~30 dB below the signal light intensity. Additionally, there is a small spike around 1030 nm observed on the left side of the spectrum's center wavelength. This spike is attributed to nonlinear effects, such as intermodal four-wave mixing. Figure 6c displays the temporal signal and the corresponding Fourier spectrum at 5030 W. At this power level, the resulting Fourier spectrum shows frequency components in the range of 0–4 kHz, as shown in the inset of Figure 6c, revealing the observation of TMI. The measured M^2 results are presented in Figure 6d at the power of 5030 W. The beam quality factors M^2 in the X-direction and Y-direction are approximately 1.57 and 1.38, respectively.

A nearly-single-mode laser output is obtained by matched fusion between fibers. The device temperature and melting point temperature in the fiber laser did not exceed 60 °C throughout the experiment.

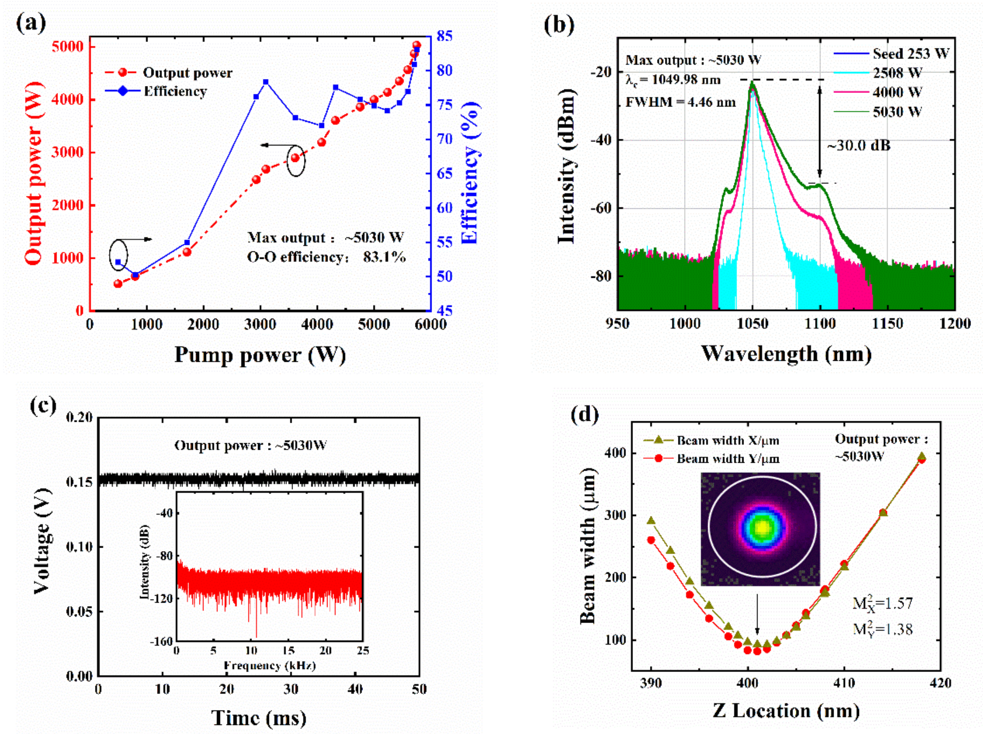

Figure 6. (**a**) Output power and conversion efficiency corresponding to different pump powers of fiber amplifier; (**b**) output spectra at different output powers; (**c**) temporal signal at 5030 W output power and the corresponding Fourier spectrum signal; (**d**) beam quality at maximum output power (inset: a beam profile of the output laser).

The application of the home-made asymmetric bi-tapered YDF allows the SRS intensity and ASE intensity in the spectrum to be controlled at a low level. From the results of this experiment, the change in the longitudinal structure of the active fiber is beneficial for the suppression of SRS, and the appropriate length and absorption coefficient of the bi-tapered YDF are beneficial for the suppression of ASE in the 1050 nm fiber laser, whereas the TMI threshold in the fiber laser is enhanced by the counter-pump structure and the optimization of working temperature of the pumping source. In the subsequent experimental study, the application of bi-tapered YDF and the integrated suppression of ASE, SRS and TMI will be an effective means to achieve high beam quality and high-power output in fiber lasers with operating wavelengths around 1050 nm.

4. Conclusions

In this study, we demonstrate a high-brightness and high-efficiency monolithic fiber laser operating at 1050 nm. By employing a specially designed asymmetric bi-tapered YDF, we achieve a nearly-single-mode laser output of 5 kW at 1050 nm. It should be noted that the current maximum power of nearly-single-mode 1050 nm fiber lasers is at the level of 3 kW. The comparison of the fiber laser constructed in this work and the fiber lasers with operating wavelengths less than 1060 nm mentioned in the manuscript is shown in Table 1. The beam quality factors at the maximum power are $M^2{}_x = 1.57$ and $M^2{}_y = 1.38$ with an O-O efficiency of 83.1%. The utilization of the asymmetric bi-tapered YDF contributes to a high SNR, reaching approximately 30.0 dB. We have successfully enhanced the TMI threshold by optimizing the working temperature of the pumping source and increasing the seed power, resulting in a higher power laser output. By further optimizing the structural parameters of the asymmetric bi-tapered YDF and fine-tuning the pump wavelength, it is possible to achieve even higher output power in fiber lasers.

Table 1. Comparison of fiber lasers with operating wavelengths less than 1060 nm.

Year	Wavelength	Output Power	M^2 Factor	Efficiency	Affiliation *	Reference
2011	1030 nm	0.697 kW		69% (Slope)	FSU Jena	[8]
2016	1034 nm	1 kW	$M^2 < 1.1$	81% (Slope)	AFRL	[9]
2016	1030 nm	1.01 kW		81% (O-O)	CAEP	[10]
2017	1032 nm	2.2 kW	$M^2 < 1.1$	40% (E-O)	IPG Photonics	[11]
2018	1030 nm	1 kW	$M^2 < 1.1$	63.8% (O-O)	CAEP	[12]
2020	1030 nm	3 kW	$M^2 < 1.2$	82% (O-O)	CAEP	[13]
2022	1030 nm	0.735 kW	$M^2 \approx 1.16$	77% (O-O)	GUT	[14]
2021	1045 nm	2.4 kW	$M^2 \approx 1.2$	80.4% (O-O)	TJU	[15]
2022	1050 nm	3.1 kW	$M^2 \approx 1.33$	75% (O-O)	NJUST	[16]
2023	1050 nm	5 kW	$M^2 \approx 1.47$	83.1% (O-O)	NUDT	

* FSU Jena: Friedrich–Schiller–Universität Jena; AFRL: Air Force Research Laboratory; CAEP: China Academy of Engineering Physics; GUT: Guilan University of Medical Sciences; TJU: Tianjin University; NJUST: Nanjing University of Science and Technology; NUDT: National University of Defense Technology; E-O: electro-optical efficiency: O-O: optical-to-optical efficiency.

Author Contributions: Conceptualization, Z.P., X.W. and F.X.; methodology, B.Y., P.W., Z.Y., Y.Y. and X.X.; validation, B.Y., Y.Y., H.Z. and Z.P.; formal analysis, H.Z., X.W. and F.X.; investigation, X.M., H.Z. and X.W.; resources, X.W., Y.Y., X.M. and B.Y.; data curation, X.M. and F.L.; writing—original draft preparation, X.M., F.L. and X.W.; writing—review and editing, X.W. and X.X.; visualization, Y.Y. and F.L.; supervision, Z.P., H.Z. and X.X.; project administration, X.X., X.W. and H.Z.; funding acquisition, X.W. and F.X. All authors have read and agreed to the published version of the manuscript.

Funding: This research was funded by the Hunan Outstanding Youth Fund, Grant No. 2023JJ10057 and the Training Program for Excellent Young Innovations of Changsha, Grant No. kq2206006, kq2206002; the National Natural Science Foundation of China, Grant No. 62005315, and Open Research Fund of State Key Laboratory of Pulsed Power Laser Technology, Electronic Countermeasure Institute, National University of Defense Technology, Grant No. SKL2022ZR02.

Data Availability Statement: Not applicable.

Acknowledgments: The authors would like to thank Jiawei Wang, Tao Song, Pengfei Zhong, Qian Yang and Xiaoyong Xu for their assistance in the whole experiment.

Conflicts of Interest: The authors declare no conflict of interest.

References

1. Augst, S.; Ranka, J.; Fan, T.; Sanchez, A. Beam combining of ytterbium fiber amplifiers (Invited). *J. Opt. Soc. Am. B* **2007**, *24*, 1707–1715. [CrossRef]
2. Fan, T.Y. Laser beam combining for high-power, high-radiance sources. *IEEE J. Sel. Top. Quant.* **2005**, *11*, 567–577. [CrossRef]
3. Kablukov, S.; Dontsova, E.; Akulov, V.; Vlasov, A.; Babin, S. Frequency doubling of Yb-doped fiber laser to 515 nm. *Laser Phys.* **2010**, *20*, 360–364. [CrossRef]
4. Chen, F.; Ma, J.; Wei, C.; Zhu, R.; Zhou, W.; Yuan, Q.; Pan, S.; Zhang, J.; Yize, W.; Dou, J. 10 kW-level spectral beam combination of two high power broad-linewidth fiber lasers by means of edge filters. *Opt. Express* **2017**, *25*, 32783–32791. [CrossRef]
5. Regelskis, K.; Hou, K.; Raciukaitis, G.; Galvanauskas, A. Spatial-dispersion-free spectral beam combining of high power pulsed Yb-doped fiber lasers. In Proceedings of the 2008 Conference on Lasers and Electro-Optics and 2008 Conference on Quantum Electronics and Laser Science, San Jose, CA, USA, 4–9 May 2008.
6. Kurkov, A.S. Oscillation spectral range of Yb-doped fiber lasers. *Laser Phys. Lett.* **2007**, *4*, 93–102. [CrossRef]
7. Tao, R.; Ma, P.; Wang, X.; Zhou, P.; Liu, Z. Study of wavelength dependence of mode instability based on a semi-analytical model. *IEEE J. Quantum Elect.* **2015**, *51*, 1–6.
8. Schmidt, O.; Wirth, C.; Rhein, S.; Rekas, M.; Kliner, A.; Schreiber, T.; Eberhardt, R.; Tunnermann, A. 697 W 12 pm linewidth of fiber generated and amplified spontaneous emission (ASE) at 1 µm. In Proceedings of the 2011 Conference on Lasers and Electro-Optics Europe and 12th European Quantum Electronics Conference, Munich, Germany, 22–26 May 2011.
9. Naderi, N.; Dajani, I.; Flores, A. High-efficiency, kilowatt 1034 nm all-fiber amplifier operating at 11 pm linewidth. *Opt. Lett.* **2016**, *41*, 1018–1021. [CrossRef]

10. Sun, Y.; Ke, W.; Feng, Y.; Wang, Y. 1030 nm Kilowatt-Level Ytterbium-Doped Narrow Linewidth Fiber Amplifier. *Chin. J. Lasers* **2016**, *43*, 0601003.
11. Platonov, N.; Yagodkin, R.; Cruz, D.; Alexander, Y.; Valentin, P. 1.5 kW linear polarized on PM fiber and 2kW on non-PM fiber narrow linewidth CW diffraction-limited fiber amplifier. *Proc. SPIE* **2017**, *100850*, 158–163.
12. Chu, Q.; Zhao, P.; Lin, H.; Liu, Y.; Wang, B.; Guo, C.; Tang, X.; Tang, C.; Jing, F. kW-level 1030 nm polarization-maintained fiber laser with narrow linewidth and near-diffraction-limited beam quality. *Appl. Opt.* **2018**, *57*, 2992–2996. [CrossRef]
13. Chu, Q.; Shu, Q.; Liu, Y.; Tao, R.; Yan, D.; Lin, H.; Wang, J.; Jing, F. 3 kW high OSNR 1030 nm single-mode monolithic fiber amplifier with a 180 pm linewidth. *Opt. Lett.* **2020**, *45*, 6502–6505. [CrossRef] [PubMed]
14. Jafari, N.; Batebi, S.; Sarikhani, S.; Chenar, R. A high power 1030 nm ytterbium doped fiber laser with a near diffraction limited quality using a 20/400 µm active fiber. *Laser Phys.* **2022**, *32*, 075103. [CrossRef]
15. Xu, Y.; Sheng, Q.; Wang, P.; Cui, X.; Zhao, Y.; Xu, H.; Ding, X.; Fang, Q.; Shi, W.; Yao, J. 2.4 kW 1045 nm narrow-spectral-width monolithic single-mode CW fiber laser by using an FBG-based MOPA configuration. *Appl. Opt.* **2021**, *60*, 3740–3746. [CrossRef] [PubMed]
16. Zheng, Y.; Han, Z.; Li, Y.; Li, F.; Wang, H.; Zhu, R. 3.1 kW 1050 nm narrow linewidth pumping-sharing oscillator-amplifier with an optical signal-to-noise ratio of 45.5 dB. *Opt. Express* **2022**, *30*, 12670–12683. [CrossRef]
17. Jauregui, C.; Limpert, J.; Tünnermann, A. High-power fibre lasers. *Nat. Photonics* **2013**, *7*, 861–867. [CrossRef]
18. Eidam, T.; Wirth, C.; Jauregui, C.; Stutzki, F.; Jansen, F.; Otto, H.; Schmidt, O.; Schreiber, T.; Limpert, J.; Tünnermann, A. Experimental observations of the threshold-like onset of mode instabilities in high power fiber amplifiers. *Opt. Express* **2011**, *19*, 13218–13224. [CrossRef]
19. Filippov, V.; Chamorovskii, Y.; Kerttula, J.; Golant, K.; Pessa, M.; Okhotnikov, O.G. Double clad tapered fiber for high power applications. *Opt. Express* **2008**, *16*, 1929–1944. [CrossRef]
20. Trikshev, A.I.; Kurkov, A.S.; Tsvetkov, V.B.; Filatova, S.A.; Kertulla, J.; Filippov, V.; Chamorovskiy, Y.K.; Okhotnikov, O.G. A 160 W single-frequency laser based on an active tapered double-clad fiber amplifier. *Laser Phys. Lett.* **2013**, *10*, 65101. [CrossRef]
21. Hejaz, K.; Shayganmanesh, M.; Roohforouz, A.; Nasirabad, R.; Abedinajafi, A.; Azizi, S.; Vatani, V. Transverse mode instability threshold enhancement in Ybdoped fiber lasers by cavity modification. *Appl. Opt.* **2018**, *57*, 5992–5997.
22. Bobkov, K.; Levchenko, A.; Kashaykina, T.; Aleshkina, S.; Bubnov, M.; Lipatov, D.; Laptev, A.; Guryanov, A.; Leventoux, Y.; Granger, G.; et al. Scaling of average power in sub-MW peak power Yb-doped tapered fiber picosecond pulse amplifiers. *Opt. Express* **2021**, *29*, 1722–1735. [CrossRef]
23. Filippov, V.; Chamorovskii, Y.; Kerttula, J.; Kholodkov, A.; Okhotnikov, O.G. 600 W power scalable single transverse mode tapered double-clad fiber laser. *Opt. Express* **2009**, *17*, 1203–1214. [CrossRef] [PubMed]
24. Zeng, L.; Wang, X.; Ye, Y.; Wang, L.; Yang, B.; Xi, X.; Wang, P.; Pan, Z.; Zhang, H.; Shi, C.; et al. High Power Ytterbium-Doped Fiber Lasers Employing Longitudinal Vary Core Diameter Active Fibers. *Photonics* **2023**, *10*, 147. [CrossRef]
25. Filippov, V.; Chamorovskii, Y.; Kerttula, J.; Kholodkov, A.; Okhotnikov, O.G. Single-mode 212 W tapered fiber laser pumped by a low-brightness source. *Opt. Lett.* **2008**, *33*, 1416–1418. [CrossRef] [PubMed]
26. Fedotov, A.; Noronen, T.; Gumenyuk, R.; Ustimchik, V.; Chamorovskii, Y.; Golant, K.; Odnoblyudov, M.; Rissanen, J.; Niemi, T.; Filippov, V. Ultra-large core birefringent Yb-doped tapered double clad fiber for high power amplifiers. *Opt. Express* **2018**, *26*, 6581–6592. [CrossRef] [PubMed]
27. Filippov, V.; Kerttula, J.; Chamorovskii, Y.; Golant, K.; Okhotnikov, O.G. Highly efficient 750 W tapered double-clad ytterbium fiber laser. *Opt. Express* **2010**, *18*, 12499–12512. [CrossRef]
28. Zeng, L.; Pan, Z.; Xi, X.; Yang, H.; Ye, Y.; Huang, L.; Zhang, H.; Wang, X.; Wang, Z.; Zhou, P. 5 kW monolithic fiber amplifier employing homemade spindle-shaped ytterbium-doped fiber. *Opt. Lett.* **2021**, *46*, 1393–1396. [CrossRef]
29. Gapontsev, D. 6 kW CW single mode ytterbium fiber laser in all-fiber format. In Proceedings of the 21st Annual Solid State and Diode Laser Technology Review, Albuquerque, NM, USA, 2–5 June 2008.
30. O'Connor, M.; Gapontsev, V.; Fomin, V.; Abramov, M.; Ferin, A. Power Scaling of SM Fiber Lasers toward 10 kW. In Proceedings of the Conference on Lasers and Electro-Optics/International Quantum Electronics Conference, Baltimore, MA USA, 31 May–5 June 2009.
31. Shcherbakov, E.; Fomin, V.; Abramov, A.; Ferin, A.; Mochalov, D.; Gapontsev, V. Industrial grade 100 kW power CW fiber laser. In Proceedings of the Advanced Solid-State Lasers Congress, Paris, France, 27 October–1 November 2013.
32. Wood, D.; Walker, K.; Macchesney, J.; Simpson, J.; Csencsits, R. Germanium chemistry in the MCVD process for optical fiber fabrication. *J. Light. Technol.* **1987**, *5*, 277–285. [CrossRef]
33. Tao, R.; Ma, P.; Wang, X.; Zhou, P.; Liu, Z. Mitigating of modal instabilities in linearly-polarized fiber amplifiers by shifting pump wavelength. *J. Opt.* **2015**, *17*, 45504. [CrossRef]
34. Wan, Y.; Xi, X.; Yang, B.; Zhang, H.; Wang, X. Enhancement of TMI Threshold in Yb-Doped Fiber Laser by Optimizing Pump Wavelength. *IEEE Photon. Technol. Lett.* **2021**, *33*, 656–659. [CrossRef]
35. Otto, H.; Stutzki, F.; Jansen, F.; Eidam, T.; Jauregui, C.; Limpert, J.; Tünnermann, A. Temporal dynamics of mode instabilities in high-power fiber lasers and amplifiers. *Opt. Express* **2012**, *20*, 15710–15722. [CrossRef]
36. Otto, H.; Jauregui, C.; Stutzki, F.; Jansen, F.; Limpert, J.; Tünnermann, A. Controlling mode instabilities by dynamic mode excitation with an acousto-optic deflector. *Opt. Express* **2013**, *21*, 17285–17298. [CrossRef] [PubMed]

37. Beier, F.; Möller, F.; Sattler, B.; Nold, J.; Liem, A.; Hupel, C.; Kuhn, S.; Hein, S.; Haarlammert, N.; Schreiber, T.; et al. Experimental investigations on the TMI thresholds of low-NA Yb-doped single-mode fibers. *Opt. Lett.* **2018**, *43*, 1291–1294. [CrossRef] [PubMed]
38. Beier, F.; Hupel, C.; Kuhn, S.; Hein, S.; Nold, J.; Proske, F.; Sattler, B.; Liem, A.; Jauregui, C.; Limpert, J.; et al. Single mode 4.3 kW output power from a diode-pumped Yb-doped fiber amplifier. *Opt. Express* **2017**, *25*, 14892–14899. [CrossRef] [PubMed]
39. Liu, W.; Ma, P.; Lv, H.; Xu, J.; Zhou, P.; Jiang, Z. General analysis of SRS-limited high-power fiber lasers and design strategy. *Opt. Express* **2016**, *24*, 26715–26721. [CrossRef]